

Diese Arbeit wurde vorgelegt am Aerodynamischen Institut

# Investigations on two-way coupling effects of particle-laden decaying isotropic turbulent flows

---

PROJEKTARBEIT  
VON  
JULIAN STEMMERMAN, STEFFEN TRIENEKENS  
UND CHRISTIAN SOIKA

---

Aerodynamisches Institut der RWTH Aachen

October 22, 2017

Betreuer: Konstantin Fröhlich  
Erstprüfer: Univ.-Prof. Dr.-Ing. Wolfgang Schröder

# Contents

|           |   |           |
|-----------|---|-----------|
| <b>I</b>  | <b>Nomenclature</b>                               | <b>2</b>  |
| <b>2</b>  | <b>Introduction</b>                               | <b>5</b>  |
| <b>3</b>  | <b>Mathematical models</b>                        | <b>7</b>  |
| 3.1       | Single phase flow . . . . .                       | 7         |
| 3.1.1     | Equations governing the fluid phase . . . . .     | 7         |
| 3.2       | Scales of turbulent flows . . . . .               | 9         |
| 3.3       | Particle dynamics . . . . .                       | 10        |
| <b>4</b>  | <b>Numerical methods</b>                          | <b>13</b> |
| 4.1       | Discretization of the particle dynamics . . . . . | 13        |
| 4.2       | Direct numerical simulation . . . . .             | 13        |
| 4.3       | Large-eddy simulation . . . . .                   | 14        |
| 4.4       | Applied simulation . . . . .                      | 14        |
| <b>5</b>  | <b>Results</b>                                    | <b>15</b> |
| 5.1       | Computational point particles . . . . .           | 15        |
| <b>6</b>  | <b>Results</b>                                    | <b>16</b> |
| <b>7</b>  | <b>Neufassung Results</b>                         | <b>19</b> |
| <b>8</b>  | <b>Conclusion and outlook</b>                     | <b>25</b> |
| <b>9</b>  | <b>References</b>                                 | <b>26</b> |
| <b>10</b> | <b>Appendix A</b>                                 | <b>28</b> |

# I Nomenclature

## Greek Symbols

|              |                          |
|--------------|--------------------------|
| $\gamma$     | Isentropic exponent      |
| $\eta$       | Kolmogorov length scale  |
| $\lambda$    | Taylor microscale        |
| $\mu$        | Dynamic viscosity        |
| $\nu$        | Kinematic viscosity      |
| $\rho$       | Fluid density            |
| $\rho_p$     | Particle density         |
| $\bar{\tau}$ | Stress tensor            |
| $\tau_\eta$  | Kolmogorov time scale    |
| $\tau_L$     | Eddy turnover time       |
| $\tau_p$     | Particle relaxation time |
| $\tau_{ps}$  | Stokes relaxation time   |
| $\psi$       | Coupling rate            |

## Operators

|          |                |
|----------|----------------|
| $\nabla$ | Nabla operator |
|----------|----------------|

## Roman Symbols

|       |                                  |
|-------|----------------------------------|
| $c_p$ | Specific isobaric heat capacity  |
| $c_v$ | Specific isochoric heat capacity |
| $d_p$ | Particle diameter                |
| $f_D$ | Drag correction                  |
| $E$   | Specific inner energy            |
| $e$   | Specific internal energy         |

|                          |  |
|--------------------------|--|
| $\boldsymbol{F}$         | Force per unitary volume of the particle acting on the fluid |
| $\boldsymbol{f}_a$       | Added mass force   |
| $\boldsymbol{f}_d$       | Drag force   |
| $\boldsymbol{f}_h$       | History force  |
| $\boldsymbol{f}_l$       | Lift force   |
| $\boldsymbol{f}^n$       | Sum of forces acting on the fluid                            |
| $\bar{\boldsymbol{H}}$   | Flux tensor  |
| $\bar{\boldsymbol{H}}^i$ | Inviscid part of the flux tensor                             |
| $\bar{\boldsymbol{H}}^v$ | Viscous part of the flux tensor                              |
| $\bar{\boldsymbol{I}}$   | Identity tensor  |
| $k_t$                    | Thermal conductivity   |
| $L$                      | Integral length scale  |
| $m_c$                    | Number of clustered particles                                |
| $N_c$                    | Number of computational particles                            |
| $N_p$                    | Number of physical particles                                 |
| $p$                      | Pressure   |
| $Pr$                     | Prandtl number   |
| $\boldsymbol{Q}$         | Vector of conservative Eulerian variables                    |
| $\boldsymbol{q}$         | Heat conduction vector                                       |
| $R$                      | Specific gas constant  |
| $Re$                     | Reynolds number  |
| $Re_p$                   | Particle Reynolds number                                     |
| $r_p$                    | Particle radius  |
| $\boldsymbol{S}$         | Rate-of-strain tensor  |
| $S$                      | Sutherland temperature                                       |

|                    |   |
|--------------------|---|
| $T$                | Temperature                                       |
| $t^*$              | Time normalized by the initial eddy turnover time |
| $\boldsymbol{u}$   | Fluid velocity                                    |
| $U$                | Characteristic fluid velocity                     |
| $V_p$              | Particle volume                                   |
| $\boldsymbol{v}_p$ | Particle velocity vector                          |
| $\boldsymbol{x}_p$ | Particle position vector                          |

## 2 Introduction

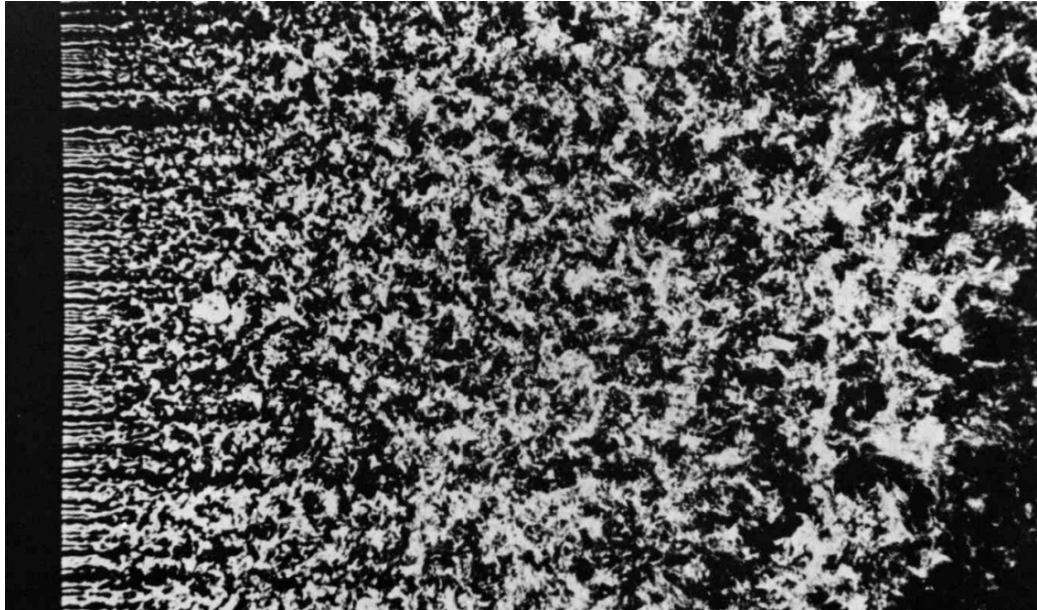


Figure 1: Photograph courtesy of Hassan Nagib and Thomas Corke: Formation of an nearly isotropic turbulent flow field behind a grid. Source: [?]

iiiiii HEAD This work deals with the effects of particles on the flow conditions of isotropic turbulent flows. There are many examples of these particle-laden turbulent flows in nature, e.g. in volcanic eruptions and in the "white water" of breaking waves.

Multiphase flows also occur in many technical applications. Spray atomization in fuel injectors, cyclonic particle separation in oil refineries and sediment accumulation in pipelines are just three of many cases, where it is of huge interest to predict the influence of particles on the turbulence of the flow. Of major industrial interest are the fuel dispersion and combustion in an petrol-powered engine. To get a homogeneous and fast combustion, both should take place at turbulent flow conditions. One could say it is an important question, in which way and intensity the particles influence the turbulence. ===== Particle laden turbulent flows are ubiquitous in nature, e.g. in volcanic eruptions and in the "white water" of breaking waves. Spray atomization in fuel injectors, cyclonic particle separation in oil refineries and sediment accumulation in pipelines are examples of technical applications, where it is of huge interest to predict the impact of particles on turbulent flows. Turbulence augmentation or attenuation by particles is therefore a decisive factor. 4113d64895656e6ba27b195eb1861d9a73879796

A study on the impact of particles on the flow conditions of isotropic turbulent

flows is presented at hand. In this work the influence of the particles on the conditions is presented. Analyzing the energy transfer between particles and fluid will be focused.

iiiiii HEAD In this work the influence of the particles on the streaming conditions is presented by using DNS and LES simulations. The focus lies on analyzing the energy transfer between particles and fluid as well as the intensity of the decrease of turbulent kinetic energy in the fluid. At the beginning some mathematical background information about modeling turbulent single phase and particle-laden flows are given. Additionally the Navier-Stokes equations and the different scales of turbulent motion are presented as an approach to modelling turbulence. For particle-laden flows the equations of motion are expanded by a new term that describes the forces acting between fluid and particles. Also the coupling rate that describes the exchanged energy and the computational basics of methods used in this work are introduced. According to the computational basics the simulation methods DNS and LES, how they work and in which case which one is used is explained. Then the used discretization method to integrate the particle tracking equations, which is a predictor-corrector-scheme, is described. Finally the computational method 'particle clustering' is introduced. This approach aims to decrease the computational effort of particle-laden simulations. It works the following way: the particles are coupled to clusters and each cluster is considered as one particle. In the following the deviations caused by using this method are determined and the applicability is evaluated. Therefore the influence of the number of particles per cluster on the accuracy of the plots of the turbulent kinetic energy and the exchanged energy between particles and fluid per time is identified. =====

First, some mathematical background information about modeling single phase and particle laden flows are given. Additionally, the scales of turbulent motion are described. According to the computational basics the simulation methods DNS and LES, how they work and in which case which one is used is explained. Then the used discretization method to integrate the particle tracking equations is described. Finally the computational method 'particle clustering' is introduced. In the following the deviations caused by using this method are determined and the applicability is evaluated. llllllll 4113d64895656e6ba27b195eb1861d9a73879796 Also the number of particles that is needed to get consistent average values for the flow characteristics is investigated.

-Due to the small particle concentration, a popular method to describe these flows is the point-particle approach, which means that every particle is treated as a mathematical point source of mass, momentum and energy.

### 3 Mathematical models

#### 3.1 Single phase flow

In this section, the mathematical models are introduced, which describe turbulent flows. For a more detailed description, see e.g. [11].

##### 3.1.1 Equations governing the fluid phase

The conservation of mass, momentum and energy for a control volume reads

$$\int_V \frac{\partial \mathbf{Q}}{\partial t} dV + \int_{\partial V} \bar{\mathbf{H}} \cdot \mathbf{n} dA = \mathbf{0}. \quad (3.1)$$

with time  $t$  and the flux tensor  $\bar{\mathbf{H}}$ . The vector  $\mathbf{Q}$  contains the variables fluid density  $\rho$ , fluid velocity  $\mathbf{u}$  and specific inner energy  $E$ :

$$\mathbf{Q} = \begin{pmatrix} \rho \\ \rho \mathbf{u} \\ \rho E \end{pmatrix}. \quad (3.2)$$

$\bar{\mathbf{H}}$  is the flux tensor which contains the inviscid and viscous flux, i.e.:

$$\bar{\mathbf{H}} = \bar{\mathbf{H}}^i + \bar{\mathbf{H}}^v = \begin{pmatrix} \rho \mathbf{u} \\ \rho \mathbf{u} \mathbf{u} + p \\ \mathbf{u}(\rho E + p) \end{pmatrix} - \frac{1}{Re} \begin{pmatrix} 0 \\ \bar{\boldsymbol{\tau}} \\ \bar{\boldsymbol{\tau}} \mathbf{u} + \mathbf{q} \end{pmatrix} \quad (3.3)$$

$\bar{\mathbf{H}}^i$  contains the variables that are independent of the fluid's viscosity and  $\bar{\mathbf{H}}^v$  represents the effects of viscosity  $\bar{\boldsymbol{\tau}}$  and heat conduction  $\mathbf{q}$ . The Reynolds number  $Re = \frac{\rho v d}{\mu}$  is defined to be the ratio of inertia forces to viscous forces. This is also due to the fact that two familiar objects with  $Re$  being identical behave similar in flows. To solve the Navier-Stokes equations, more information regarding some variables is required. For calculating the specific inner energy  $E$  and the heat conduction  $\mathbf{q}$ , the following equations are used

$$E = e + \frac{1}{2} |\mathbf{u}|^2, \quad (3.4)$$

$$\mathbf{q} = -\frac{\mu}{Pr(\gamma - 1)} \nabla T, \quad (3.5)$$

with

$$\gamma = \frac{c_p}{c_v} \quad (3.6)$$



and the Prandtl number  $Pr = \frac{\mu_\infty c_p}{k_t}$  using the specific heat capacities of the fluid  $c_v$  and  $c_p$ . Assuming that the fluid is a newtonian fluid, the linear correlation between stress and the rate of strain results in:

$$\bar{\tau} = 2\mu\bar{S} - \frac{2}{3}\mu(\nabla \cdot \mathbf{u})\bar{I}, \quad (3.7)$$

in which  $\bar{S} = \frac{(\nabla \mathbf{u})(\nabla \mathbf{u})^T}{2}$  denotes the rate-of-strain tensor. Additionally, the viscosity  $\mu$  can be approximated by Sutherland's law, which is based on the ideal gas-theory

$$\mu(T) = \mu_\infty \left( \frac{T}{t_\infty} \right)^{3/2} \frac{T_\infty + S}{T + S}, \quad (3.8)$$

where  $S$  is the Sutherland temperature. To achieve closure the caloric state equation  $e = c_v T$  and the state equation for an ideal gas  $p = \rho R T$  are used. The specific gas constant is determined by  $R = c_p - c_v$ .

### 3.2 Scales of turbulent flows

Turbulent flows contain eddies, which are induced by reverse currents in the flow, of all sizes and shapes. Large-scale eddies bring energy to the flow which is then passed down to smaller-scales, and finally dissipated into heat by viscous effects. This behavior is called the 'energy cascade' and was first described by Richardson in the year 1920 [13]. The theory then was further developed by Kolmogorov [9]. The main difference is that Kolmogorov added hypotheses like the statistical isotropy of small-scale turbulent motions and the decrease of the velocity and timescales with the decrease of the length scale along the energy cascade.

The first set of scales describe the large eddies. At these scales the energy is brought into the flow, creating the 'energy-containing range'. The corresponding timescale, which is most times called 'eddy turnover time', is defined as

$$\tau_L = \frac{L}{U}, \quad (3.9)$$

with the length scale  $L$  and the characteristic fluid velocity  $U$ .

The smallest scales in a turbulent flow are the Kolmogorov length ( $\eta$ ) and time ( $\tau_\eta$ ) scale. At these scales, the effects of viscosity take place and the energy dissipates into heat. With the estimate  $\epsilon \approx \frac{U^3}{L}$  they can be written as

$$\eta = \left( \frac{\nu^3 L}{U^3} \right)^{1/4}, \quad (3.10)$$

$$\tau_\eta = \left( \frac{\nu L}{U^3} \right). \quad (3.11)$$

Both these scales are coupled by the Reynolds numbers

$$\frac{L}{\eta} = Re^{3/4}, \quad (3.12)$$

$$\frac{\tau_L}{\tau_\eta} = Re_L^{1/2}. \quad (3.13)$$

It can be observed from these equations that the spacing between the scales increases for higher Reynolds numbers.

A scale between these two is the Taylor microscale, often referred to as 'turbulence length scale'. It is often used to describe the intermediate range between integral and Kolmogorov scales. This scale's definition is:

$$\lambda = \sqrt{15 \frac{\nu}{\epsilon}} |\mathbf{u}'| \quad (3.14)$$

with  $|\mathbf{u}'|$  denoting the absolute value of the velocity's fluctuation. This scale can be used to compute the Taylor-scale Reynolds number  $Re_\lambda$ :

$$Re_\lambda = \frac{|\mathbf{u}'| \lambda}{\nu}. \quad (3.15)$$

### 3.3 Particle dynamics

This work deals with particle-laden fluids, therefore the interaction between particles and the carrier fluid needs to be considered in the dynamic equation of both media. The phenomenon is called two-way-coupling.

In this thesis, small and heavy rigid particles with a spherical shape in an incompressible fluid are regarded. Their diameter  $d_p$  is even smaller than the Kolmogorov scale  $\eta$ , but also large enough to neglect the Brownian motion.

Due to the low particle concentration, a popular method to describe these flows is the Lagrangian point-particle approach, which means that every particle is treated as a mathematical point source of mass, momentum and energy. In this case the focus lies on the momentum exchange, effects like particle collision as well as mass exchange over the particle surface and gravity are neglected. To take the forces acting from the particles on the fluid into account the Navier-Stokes equation for the carrier fluid "Gleichung xy" is extended by the force  $\mathbf{F}$  that acts on the ambient cells with different intensity regarding on the distance between these cells and the particle:

$$\mathbf{F} = \mathbf{F}_{pp} \cdot \frac{e^{-(d_i^2/(\sigma\Delta^2))}}{\sum_i e^{-(d_i^2/(\sigma\Delta^2))}}, \quad (3.16)$$

with the distance between particle position and midpoint of the cell  $d_i$ , the length of the cells  $\Delta$  and a smoothing parameter  $\sigma$  that controls the distribution of  $\mathbf{F}$  on the adjacent cells. In this work a  $\sigma$  value of 4 was used.  $\mathbf{F}_{pp}$  is the sum of pressure and shear forces acting on the particles and is described explicit in the Maxey Riley equation that can be achieved from [?].  $\mathbf{F}_{pp}$  could be divided into several forces. Reduced to the governing forces acting on the particles the dynamic equation of the particles becomes

$$\mathbf{F}_{pp} = m_p \frac{d\mathbf{v}_p}{dt} = \rho V_p \frac{D\mathbf{u}}{Dt} - \frac{3}{4} \rho V_p \frac{C_d}{d_p} |\mathbf{v}_p - \mathbf{u}| (\mathbf{v}_p - \mathbf{u}) + \frac{1}{2} \rho V_p \left( \frac{D\mathbf{u}}{Dt} - \frac{d\mathbf{v}_p}{dt} \right) + \frac{3}{2} d_p^2 \rho \sqrt{\pi \nu} \int_{t_0}^t \frac{dt'}{(t - t')^{1/2}} \left( \frac{D\mathbf{u}}{Dt'} - \frac{d\mathbf{v}_p}{dt'} \right). \quad (3.17)$$

$\mathbf{v}_p(\mathbf{x}_p, t)$  is the particle velocity vector with the time derivative  $d/dt$  following a sphere while  $D/Dt$  is the time derivative following a fluid unit. The individual forces on the right side of the equation are stated in the following:

- $\rho V_p \frac{D\mathbf{u}}{Dt}$ :  
pressure gradient of the undisturbed flow

- $-\frac{3}{4}\rho V_p \frac{C_d}{d_p} |\mathbf{v}_p - \mathbf{u}|(\mathbf{v}_p - \mathbf{u})$ :  
hydrodynamical drag force that is parallel to the undisturbed streamlines, which depends on an empirical drag coefficient  $C_d$  defined by Schiller and Naumann as  $C_d = \frac{24}{Re_p}(1 + 0.15Re_p^{0.687})$ .
- $\frac{1}{2}\rho V_p \left( \frac{D\mathbf{u}}{Dt} - \frac{d\mathbf{v}_p}{dt} \right)$ :  
added mass force, that represents the influence of the fluid's inertia that has an impact on the particle, if it has a different acceleration than the particles
- $\frac{3}{2}d_p^2\rho\sqrt{\pi\nu} \int_{t_0}^t \frac{dt'}{(t-t')^{1/2}} \left( \frac{D\mathbf{u}}{Dt'} - \frac{d\mathbf{v}_p}{dt'} \right)$ :  
history force taking diffusion and convection into account that results from vortices slipstream

As presented by Vincenzo Armenio and Virgilio Fiorotto [?] compared to the Stokes drag all other forces could be neglected with rising particle density, so due to the density relation  $\rho_p/\rho \gg 1$ ,  $\mathbf{F}_{pp}$  can be approximately reduced to the dominating viscous drag.(3.17) becomes

$$\mathbf{F}_{pp} = m_p \frac{d\mathbf{v}_p}{dt} = \frac{3}{4}\rho V_p \frac{C_d}{d_p} |\mathbf{v}_p - \mathbf{u}|(\mathbf{v}_p - \mathbf{u}). \quad (3.18)$$

Using the particle Reynolds number  $Re_p = \frac{v_r d_p}{\nu}$  with the relative velocity between particle and fluid  $v_r$ , (3.18) can be compressed, which is described in detail in [12].

$$\rho_p \frac{d\mathbf{v}_p}{dt} = \rho_p \frac{\mathbf{v}_p - \mathbf{u}}{\tau_p} f_d. \quad (3.19)$$

Here the particle response time  $\tau_p = \frac{(\rho_p/\rho)d^2}{18\nu}$  is introduced which is a time constant in the exponential decay of the particle velocity as a result of an upcoming fluid drag and physically represents the time scale over which the drag force decreases the particle's relative velocity to zero.  $f_d = 1 + 0.15Re_p^{0.687}$  is a correction factor depending on the flow conditions.

Together with the kinematic equation of a particle

$$\frac{d\mathbf{x}_p}{dt} = \mathbf{v}_p, \quad (3.20)$$

the equations -Gl main flow- and (3.17) form the basic equations for the particle laden system.

---

In results: The coupling rate  $\psi$ , that describes the transferred energy per time between particles and fluid, is defined as

$$\psi = \mathbf{F} \cdot \mathbf{u}. \quad (3.21)$$

Hence it results from the force per unitary volume exerted between the fluid and the particles and the main velocity of the fluid. It is an useful variable to describe how much the main fluid and the particles influence each other.

## 4 Numerical methods

Two numerical methods are discussed and their main differences pointed out in the following chapter, the DNS (direct numerical simulation) and the LES (large-eddy simulation). The basis of both are the Navier-Stokes equations as described above.

### 4.1 Discretization of the particle dynamics

To integrate the Lagrangian particle tracking equations, discussed above, a predictor-corrector scheme based on the trapezoidal rule for numerical integration

$$f(t + \delta t) \approx f(t) + \frac{\delta t}{2} \left[ \frac{\partial f(t)}{\partial t} + \frac{\partial f(t + \delta t)}{\partial t} \right] \quad (4.1)$$

is used.

The first step is the prediction of the new particle position  $\mathbf{x}_{p,n+1}$  using a Taylor expansion for a small time step  $\delta t$

$$\mathbf{x}_{p,n+1} = \mathbf{x}_{p,n} + \delta t \mathbf{v}_{p,n} + \frac{1}{2} \delta t^2 \mathbf{a}_{p,n}, \quad (4.2)$$

with  $\mathbf{a}_{p,n}$  particle acceleration.

To avoid filtering effects, we will set the fluid velocity  $\mathbf{u}(\mathbf{x}_{p,n+1})$  at the particle position  $\mathbf{x}_{p,n+1}$  equal to the nearest cell fluid velocity.

The updated velocity and acceleration are calculated as

$$\mathbf{v}_{p,n+1} = \frac{\mathbf{v}_{p,n} + \frac{1}{2} \delta t \left( \mathbf{a}_{p,n} + \frac{f_D}{\tau_p} \mathbf{u}(\mathbf{x}_{p,n+1}) \right)}{1 + \frac{1}{2} \frac{f_D}{\tau_p} \delta t}, \quad (4.3)$$

$$\mathbf{a}_{p,n+1} = \frac{\frac{f_D}{\tau_p} (\mathbf{u}(\mathbf{x}_{p,n+1}) - \mathbf{v}_{p,n}) - \frac{1}{2} \delta t \mathbf{a}_{p,n}}{1 + \frac{1}{2} \frac{f_D}{\tau_p} \delta t}. \quad (4.4)$$

The updated particle position must be corrected by an additional term according to the trapezoidal rule

$$\mathbf{x}_{p,n+1} = \mathbf{x}_{p,n} + \frac{1}{2} \delta t (\mathbf{v}_{p,n+1} + \mathbf{v}_{p,n}) + \frac{1}{12} \delta t^2 (\mathbf{a}_{p,n+1} - \mathbf{a}_{p,n}). \quad (4.5)$$

### 4.2 Direct numerical simulation

With DNS, the Navier-Stokes equations are solved completely. This provides a very accurate result, as all scales of motion are being resolved. Still it requires an immense level of computational resources which increases rapidly with the Reynolds number:  $N^3 \propto 4.4 Re_L^{9/4} \approx 0.06 Re_\lambda^{9/2}$  with  $N$  size of the simulation. These computational resources were not available until the 1970s. With the LES,

as described below, the computational effort is 99.98 % less compared to DNS, which indeed is the fraction of the dissipative scale. This leaves 0.02 % of the flow, which is correlative with the fraction of the energy-containing larger-scale [11].

### 4.3 Large-eddy simulation

Due to the fact that DNS is effortful, LES was created to save time and resources. The energy containing larger-scale motion is completely resolved and the small effects of the smaller-scale motion are just modeled. Otherwise in DNS resolving the small dissipative scale would require most of the computational resources.

Simulating only the larger-scale motions is called filtering, which means that the smaller-scale motions, also known as fluctuation, are filtered out.  $\int_{-\infty}^{\infty} \frac{\partial \mathbf{Q}}{\partial t} dV + \int_{\partial V} \bar{\mathbf{H}} \cdot \mathbf{n} dA = \mathbf{0}$  For further information on filter functions, the works of Pope [11] should be considered. To model the filtered smaller-scale motions usually a subgrid-scale (SGS) model is used. According to Hickel (2007) the interference between explicit SGS and the truncation error can be exploited, i.e. the truncation error can serve as model of the effects of unresolved scales, which is therefore an implicit SGS model. Thus we call it implicit LES (ILES) [6].

### 4.4 Applied simulation

The simulations were carried out using ZFS, the simulation tool developed and implemented at the Institute of Aerodynamics at RWTH Aachen University [1] [2]. The tool is capable of simulating finite-volume flows of compressible fluids. In the simulations, which results the reader can see at hand, the Mach-number  $Ma$  was set to 0.1 to simulate an almost incompressible fluid.

## 5 Results

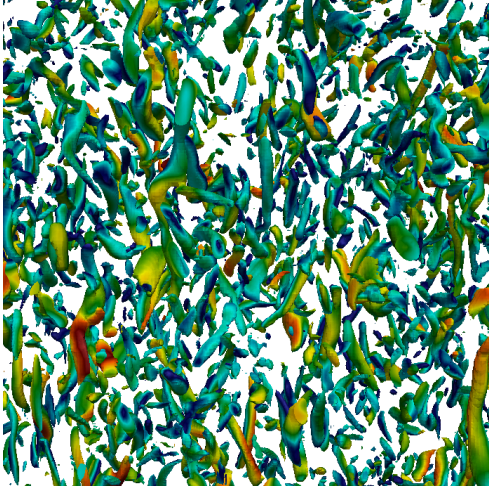


Figure 2: ???

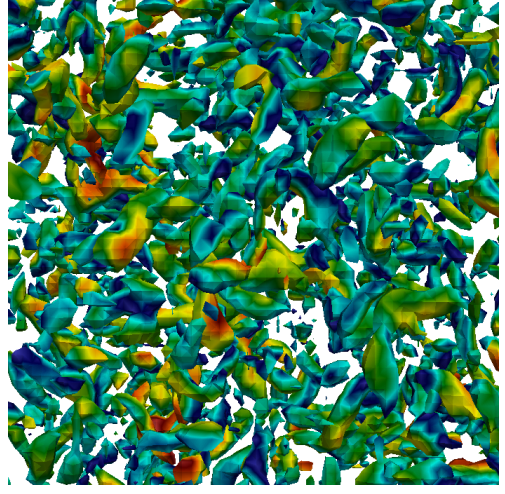


Figure 3: ??? Appendix A

iiiiiii HEAD Simulating only the larger-scale motions is called filtering, which means that the smaller-scale motions, also known as fluctuation, are filtered out. For further information on filter functions, the works of Pope [11] should be considered. To model the filtered smaller-scale motions usually a subgrid-scale (SGS) model is used. According to Hickel (2007) the interference between explicit SGS and the truncation error can be exploited, i.e. the truncation error can serve as model of the effects of unresolved scales, which is therefore an implicit SGS model. Thus we call it implicit LES (ILES) [6].

### 5.1 Computational point particles

The high number of point particles requires even more computational resources for the particle-laden simulations than for the single-phase simulations. The main idea to reduce this requirement is to create clusters of point particles. For this purpose the ratio  $\lambda_c$  of physical point particles  $N_p$  to computational point particles  $N_c$  is introduced ( $\lambda_c = \frac{N_p}{N_c}$ ). To compensate this lack of particles, the coupling force is multiplied by  $\lambda_c$ , due to the  $\lambda_c$ -fold mass of the (cluster-)particles.



## 6 Results

With the aim of more efficient computational effort for simulating the particle-laden flow while still achieving high quality results, a clustering of particles was implemented. For this purpose, the variable  $\lambda_c$  was introduced to the code describing the number of particles in one cluster, leading to the results at hand. The simulations were then set up with the overall same number of a million particles, altering just the number of particles in one cluster. These simulations result in the graphs included in this work. ===== The turbulent flow was simulated on a cartesian grid of a cubic domain using  $64^3$ ,  $96^3$ ,  $128^3$  and  $256^3$  grid points. As a consequence of missing smaller scales and therefore the utilization of a subgrid-scale model the first three cases were simulated using LES. The  $256^3$ -case is capable of portraying these, it is therefore a direct numerical simulation.

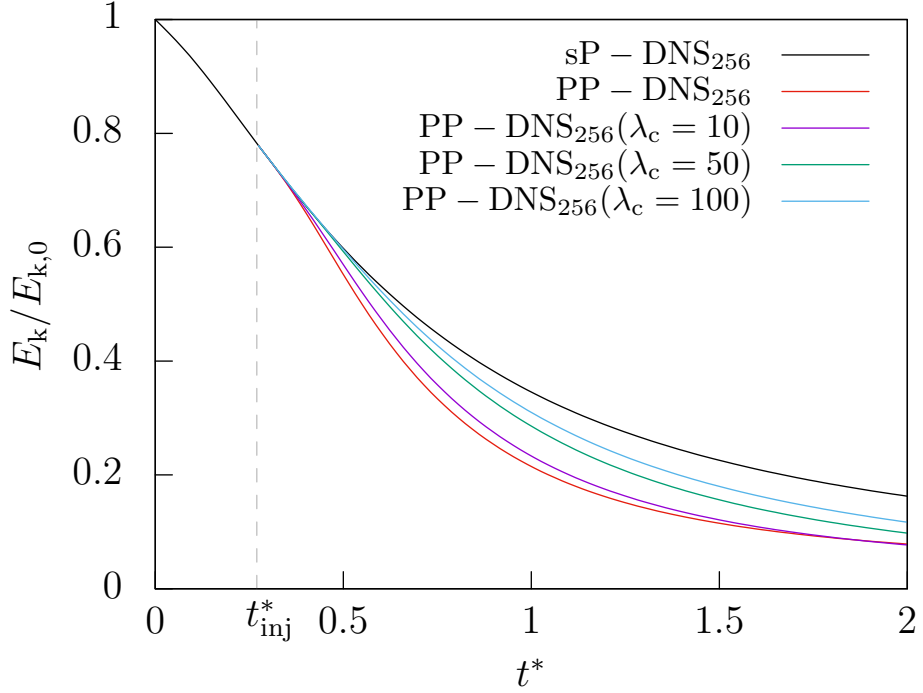


Figure 4: Kinetic energy  $E_k$  normalized by initial value of particle-free case  $E_{k,0}$  as a function of time normalized by initial eddy turnover time for different numbers of clustered particles with fixed all-over particle number. The injection time is marked by  $t_{inj}^*$ , particle-free case by (s.p.), particle-laden cases by (p.l.) enhanced with number of grid points and ratio of physical to computational particles  $m_c$ . A faster dissipation of turbulent kinetic energy can be seen for particle-laden cases in regard to the particle-free case due to additional dissipation induced by the particle-load.

For simplification, the special case of isotropic turbulence was used. For this idealized flow form the statistical velocities are invariant in all directions of the grid.

It follows that the flow velocity is also invariant for rotations and reflections. The turbulence was initialized using a seed-based random generator. To achieve physical results, the simulation of the particle-free flow was carried out a reasonable amount of time, at which a restart file was written out. This procedure ensures a fully developed turbulent flow, which has emancipated from the initialization. In this flow field, a specific number of spherical point-particles were injected.

With the aim of more efficient computational effort for simulating the particle-laden flow while still achieving high quality results, a clustering of particles was implemented. For this purpose, the variable  $m_c$  was introduced to the code describing the number of particles in one cluster, leading to the results at hand. The simulations were then set up with the overall same number of a million particles, altering just the number of particles in one cluster. These simulations result in the graphs included in this work. `lllllll 777fd7346428bdf4f18098d693bb9c4bf9d390a2` It can be seen in Fig. 7 that the decay in kinetic energy from the starting point depends highly on the number of clustered particles. `iiiiiii HEAD =====` Fitting to this first results, the Graphs of Fig. 6 and ?? clearly show that for simulations with a high rate of physical point particles to computational point particles the results differ significantly from unclustered simulations. Looking at the results for the change in kinetic energy, the difference becomes evident: The higher  $\lambda_c$  is, the lower is the drop in rate of change of the kinetic energy. It approaches more and more the particle free case.

**The particles therefore have two effects on the fluid: Firstly, the viscous dissipation rises in the case of particle-load. Secondly, there is always an energy transfer from the particles to the surrounding fluid. Both of these effects influence the kinetic energy and an equality in the energy balance for the particles can be observed at about one eddy turnover time for the unclustered simulation. At this point in time the rate of kinetic energy flowing from the particles to the fluid matches the *additional* rate of dissipated energy induced by the particles.**

The results by Schneiders et al. [10] show that for particles with constant diameter this point is reached later in time for more dense particles due to their inertia. It could be observed a similar effect with the simulation presented here: The more particles are summarized in one cluster, the later the balanced state of energy flow and dissipation is achieved. From this point on, the kinetic energy drops slower than in the particle-free case.

In difference to the others, the case in which many particles were clustered show a different behavior in this thesis. It catches up to the particle-free case very fast,

which leads to the conclusion that the amount of clusters is so small that the flow almost behaves like one without particles. Additionally, the change in kinetic energy shows inconstancy which can also be traced back to the small number of clusters. The amount is just too small to achieve high-quality information in the statistical variables.

The same impression can be achieved by analyzing the graphs describing the coupling rate (Fig. ??). The particle-laden case makes the biggest jump into negative coupling rate. The higher the number of clustered particles, the lower is the amount of the coupling rate. At high values for  $\lambda_c$  the simulations start to show remarkable differences.

Being very similar in the time shortly after the injection, the flow statistics diverge more and more when time passes by. The variables of these simulations one turnover time after the injection can be found in table 1.

To find out at which number of particles the results are sufficiently exact, a second set of simulations was carried out. As mathematical description of turbulent flows is based on statistics, small numbers of particles can lead to questionable results. **In these simulations, no particle clustering was used, just different numbers of particles were injected into the same flow. For these simulations similar properties to the ones from the first set of simulations were used, just the mentioned number of particles was changed.** An example for the deviation in kinetic energy for different numbers of particles can be found in Fig. 11.

The normalized difference in kinetic energy  $E_{kB}$  of the particles and the flow itself  $E_k$  shows in this single simulation a correlation between particle number and accuracy in the simulation. Although this was just a single initialization of particles in a flow, it can be stated that simulations using only  $10^2$ ,  $10^3$  or even up to  $10^4$  particles are not accurate enough for technical or scientific use of data. Simulations in other grid sizes show similar results.

## 7 Neufassung Results

### 1. Simulation Properties & Assumptions

In this section the results of the performed simulation will be pointed out with special emphasis on turbulent kinetic energy budgets and their influence on particle-laden turbulent flows.

All cases were simulated on a cubic domain and a cartesian grid using multiple grid refinement levels,  $64^3$ ,  $96^3$  and  $128^3$  representing the LES hence the need to model smaller scales with SGS-models is present. Due to higher grid refinement in the  $256^3$ -case, these smaller scales can be directly simulated and therefore this simulation is a DNS.

The particle-free case was initialized using a seed-based random generator. At  $t^* \approx 0.27$  a restart file is written out to initialize the subsequent simulation of the particle-laden isotropic turbulence. This file is then used to set up a second simulation including particle-load. Both these cases, DNSs of a single-phase and a particle-laden flow will be used as reference for analyzing other results. Single-phase simulations will in the following be referred to as sP, and particle-laden ones as PP. The PP-simulation was set up to match the volume fraction  $\phi_v = 10^{-3}$  and mass fraction of  $\phi_m = 1$ . Both were constant in all simulations regarding particle clustering. The ratio of the densities for this set of simulations was set to  $\frac{\rho_p}{\rho} = 1000$ , the particle diameter was set to match  $d_p \approx 0.6\eta$ . The injection of a million spherical point-particles was carried out interpolating the velocities of the surrounding fluid. At the timestep of injection the Stokes response time  $\tau_{ps}$  was 0.03497, the Prandtl number was 0.72 and  $Re_\lambda$  was 57.9757.

### 3. Turbulent kinetic Energy budgets (Schneiders)

The change in kinetic energy of the fluid is in particle-laden decaying isotropic turbulence determined by the coupling rate  $\Psi$ , which describes the energy transfer between both fluid and particle phase, and the integral dissipation rate  $\epsilon$ :

$$\frac{\partial E_k}{\partial t} = \Psi(t) - \epsilon(t). \quad (7.1)$$

As mentioned before, the flow field is considered nearly incompressible, therefore the equation for the viscous dissipation rate can be approximated by

$$\epsilon(t) \approx 2\mu \bar{\mathbf{S}} : \bar{\mathbf{S}}, \quad (7.2)$$

where  $:$  denotes the inner tensor product. This rate can then be integrated over the full fluid domain  $\Upsilon_f$ , leading to

$$\epsilon(t) = \int_{\Upsilon_f} \epsilon(t) dV. \quad (7.3)$$

As the dissipation rate is always of positive value, it acts a sink for the fluid's turbulent kinetic energy. In difference to that, the coupling rate can serve either as source or sink, depending on the acceleration of the particles [?]. The coupling rate for point-particles is defined as

$$\Psi(t) = \sum_{p=1}^{N_p} \psi_p = - \sum_{p=1}^{N_p} \mathbf{F}_p \bullet \mathbf{v}_p, \quad (7.4)$$

describing the transfer of kinetic energy resulting from surface forces at each particle.

$$\frac{dE_{kB}}{dt} = -\Psi(t) \quad (7.5)$$

therefore is the rate of change for global kinetic energy of the particles. Additionally the particles change the fluid's rate of dissipation  $\epsilon$  due to their volume forces.

## 5. Ungenauigkeits-Plot

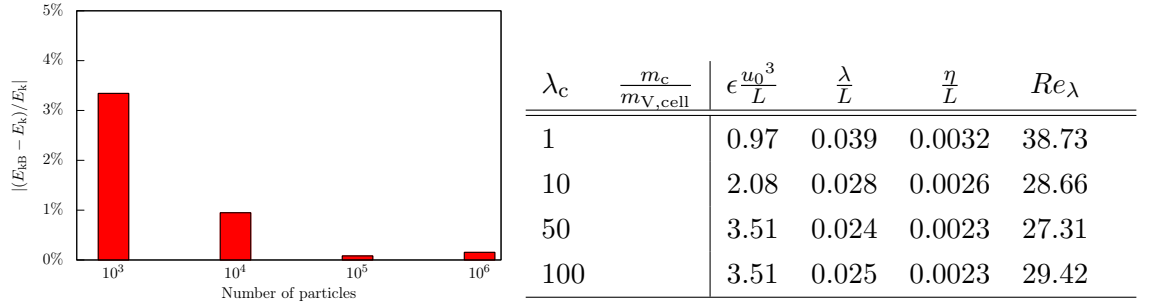


Figure 5: ???

## 6. Plots von Ek und dE

6a85c6ef33dd2a664dfbe4d0e3b91ae8baf762aa

HEAD Fitting to this first results, the Graphs of Fig. 6 and ?? clearly show that for simulations with a high rate of physical point particles to computational point particles the results differ significantly from unclustered simulations. Looking at the results for the change in kinetic energy, the difference becomes evident: The higher  $m_c$  is, the lower is the drop in rate of change of the kinetic energy. It approaches more and more the particle free case.

**The particles therefore have two effects on the fluid: Firstly, the viscous dissipation rises in the case of particle-load. Secondly, there is always an energy transfer from the particles to the surrounding fluid. Both of these effects influence the kinetic energy and an equality in the energy balance for the particles can be observed at about one eddy turnover**

time for the unclustered simulation. At this point in time the rate of kinetic energy flowing from the particles to the fluid matches the *additional* rate of dissipated energy induced by the particles. ===== 7.

Plot für Dissipation und Coupling Rate

~~~~~ 6a85c6ef33dd2a664dfbe4d0e3b91ae8baf762aa

The results by Schneiders et al. [10] show that for particles with constant diameter this point is reached later in time for more dense particles due to their inertia. It could be observed a similar effect with the simulation presented here: The more particles are summarized in one cluster, the later the balanced state of energy flow and dissipation is achieved. From this point on, the kinetic energy drops slower than in the particle-free case.

In difference to the others, the case in which many particles were clustered show a different behavior in this thesis. It catches up to the particle-free case very fast, which leads to the conclusion that the amount of clusters is so small that the flow almost behaves like one without particles. Additionally, the change in kinetic energy shows inconstancy which can also be traced back to the small number of clusters. The amount is just too small to achieve high-quality information in the statistical variables.

~~~~~ HEAD The same impression can be achieved by analyzing the graphs describing the coupling rate (Fig. ??). The particle-laden case makes the biggest jump into negative coupling rate. The higher the number of clustered particles, the lower is the amount of the coupling rate. At high values for  $m_c$  the simulations start to show remarkable differences.

Being very similar in the time shortly after the injection, the flow statistics diverge more and more when time passes by. The variables of these simulations one turnover time after the injection can be found in table 1.

| $m_c$ | $\epsilon \frac{u_0^3}{L}$ | $\frac{\lambda}{L}$ | $\frac{\eta}{L}$ | $Re_\lambda$ |
|-------|----------------------------|---------------------|------------------|--------------|
| 1     | 0.97                       | 0.039               | 0.0032           | 38.73        |
| 10    | 2.08                       | 0.028               | 0.0026           | 28.66        |
| 50    | 3.51                       | 0.024               | 0.0023           | 27.31        |
| 100   | 3.51                       | 0.025               | 0.0023           | 29.42        |

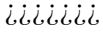
Table 1: Variables of the first set of simulations one turnover time after injection for the  $256^3$ -case

To find out at which number of particles the results are sufficiently exact, a second set of simulations was carried out. As mathematical description of turbulent

flows is based on statistics, small numbers of particles can lead to questionable results. **In these simulations, no particle clustering was used, just different numbers of particles were injected into the same flow. For these simulations similar properties to the ones from the first set of simulations were used, just the mentioned number of particles was changed.** An example for the deviation in kinetic energy for different numbers of particles can be found in Fig. 11. The normalized difference in kinetic energy  $E_{kB}$  of the particles and the flow itself  $E_k$  shows in this single simulation a correlation between particle number and accuracy in the simulation. Although this was just a single initialization of particles in a flow, it can be stated that simulations using only  $10^2$ ,  $10^3$  or even up to  $10^4$  particles are not accurate enough for technical or scientific use of data. Simulations in other grid sizes show similar results. =====

9. Plot fuer kinetische Energie der Partikel und Vergleichsplot DNS i- LES (Coupling Rate)

11. Erklärung aller Plots mittels kinetic energy budget

12. Computational savings  6a85c6ef33dd2a664dfbe4d0e3b91ae8baf762aa

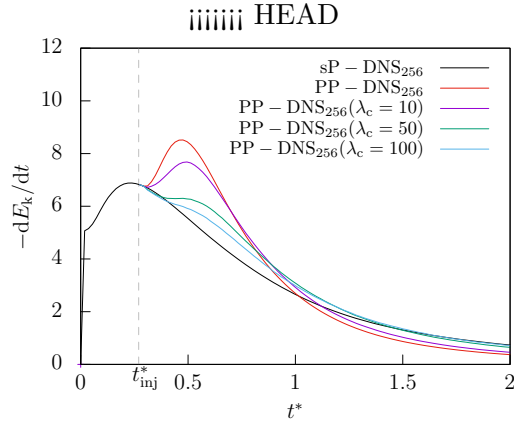


Figure 6: Change in **normalized** turbulent kinetic energy over time normalized by eddy turnover time: The particle-laden cases show higher rates of dissipation after the injection and lower rates later in time. This effect becomes smaller for higher numbers of clustered particles.

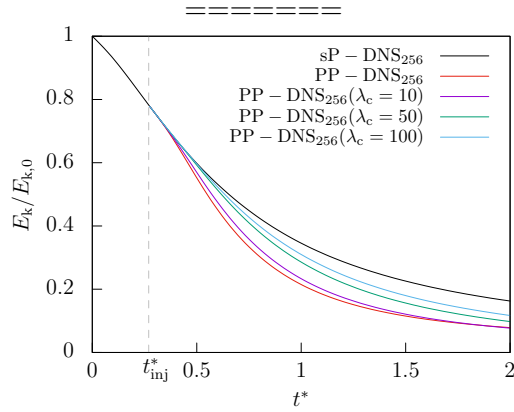


Figure 7: ???

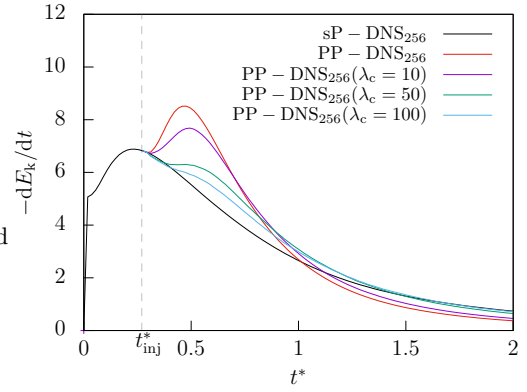


Figure 8: ???

6a85c6ef33dd2a664dfbe4d0e3b91ae8baf762aa



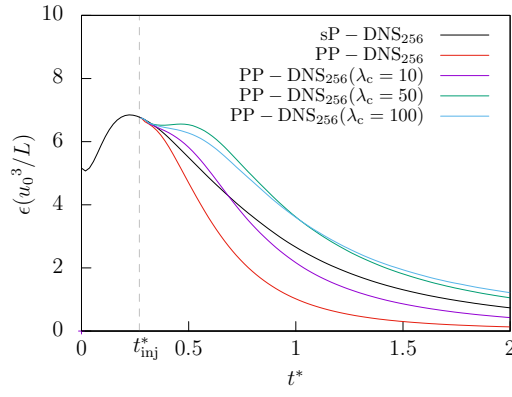


Figure 9: ???

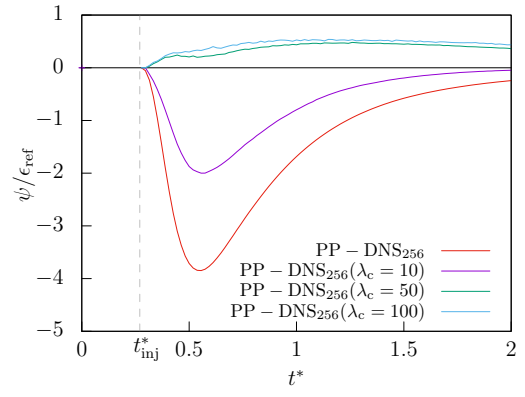


Figure 10: ???

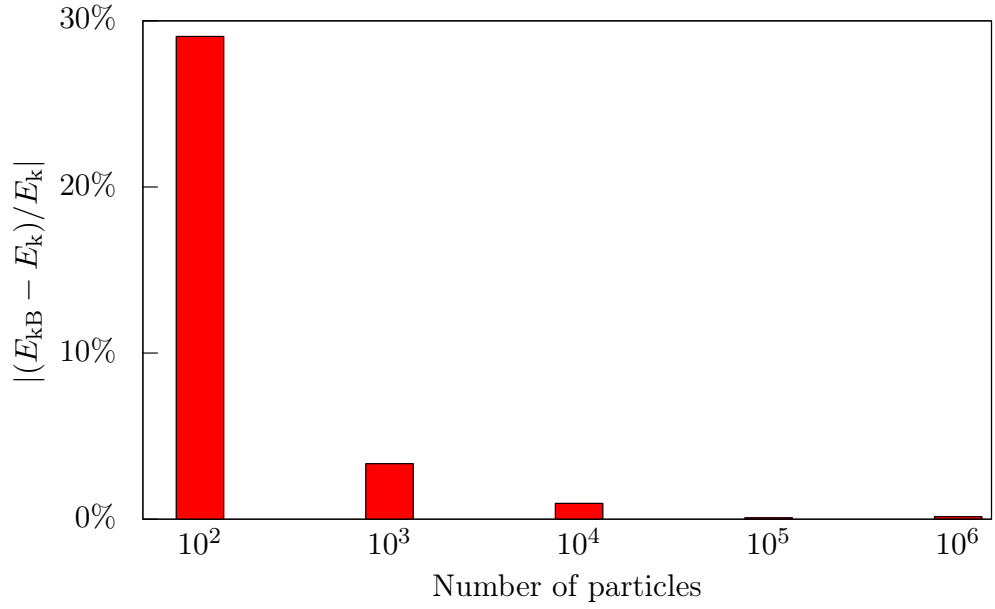


Figure 11: Results for initializing different numbers of particles

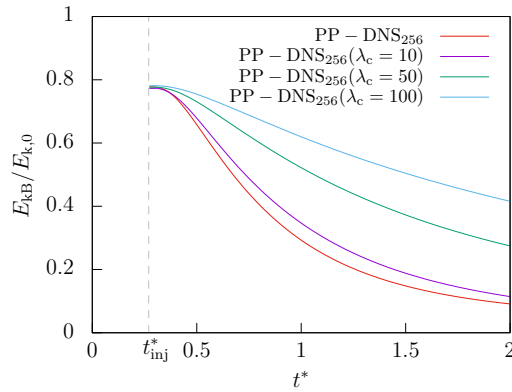


Figure 12: ???

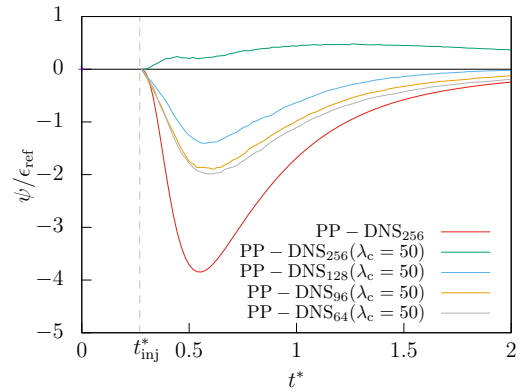


Figure 13: ???

## 8 Conclusion and outlook

In this work, two sets of simulations were carried out to evaluate a method for lowering computational effort.

The results presented in this work show, that for a sufficiently exact simulation, particle clustering has to be treated with caution. Depending on the application maybe small numbers of clustered particles could be used, but the savings in computing time would not compensate the loss in accuracy. This is the case in particular high numbers of clustered particles at which the results get highly inaccurate. Maybe investigations on smaller numbers of clustered particles could follow, the space between 2 and 10 could be closed by simulations in the future to determine the real border for inaccurate results.

Further investigation is needed regarding the second set of simulation, in which the goal was to find out which number of particles is necessary to get accurate results for the turbulent kinetic energy of the particles. The deviation of the averaged kinetic energy of the particles and the fluid should be zero. This difference converges to zero with high numbers of particles. The distribution of the experiment's outcomes should match the well-known normal distribution, which leads to analyzing the standard deviation. Concluding, further simulations should be carried out until a sufficient standard deviation can be computed, from which an assumption about the accuracy of the initialization could be made.

## Acknowledgements

This work was supervised by Konstantin Fröhlich, we would like to express our gratitude. Thank you for the chance of learning about turbulent flows and simulations, the advice and the deep insights in scientific work. We also appreciate the chance of writing this work at the Institute of Aerodynamics of the RWTH Aachen University.

## 9 References

- [1] W. Schröder D. Hartmann, M. Meinke. An adaptive multilevel multigrid formulation for cartesian hierarchical grid methods. *Comput. Fluids*, 2008.
- [2] W. Schröder D. Hartmann, M. Meinke. A strictly conservative cartesian cut-cell method for compressible viscous flows on adaptive grids. *Comput. Meth. Appl. Mech. Eng.*, 2010.
- [3] S. Elghobashi. Particle-laden turbulent flows: direct simulation and closure models. *Applied Scientific Research*, 1991.
- [4] S. Elghobashi. On predicting particle-laden turbulent flows. *Applied Scientific Research*, 1993.
- [5] S. Fritz. Simulation isotroper turbulenz. study work, 2003.
- [6] S. Hickel. *Implicit Turbulence Modeling for Large-Eddy Simulation*. PhD thesis, Technische Universität München, 2007.
- [7] John K. Eaton John R. Fessler, Jonathan D. Kulick. Preferential concentration of heavy particles in a turbulent channel flow. *Physics of Fluids*, 1994.
- [8] M. Meinke K. Fröhlich, L. Schneiders and W. Schröder. Validation of particle-laden large-eddy simulation using hpc systems. In *Sustained Simulation Performance 2017*, 2017. unpublished conference document.
- [9] A. Kolmogorov. The local structure of turbulence in incompressible viscous fluid for very large reynolds' numbers. *Doklady Akademiia Nauk SSSR*, 1941.
- [10] Wolfgang Schröder Lennart Schneiders, Matthias Meinke. Direct particle-fluid simulation of kolmogorov-length-scale size particles in decaying isotropic turbulence. *Journal of Fluid Mechanics*, 2017.
- [11] S. B. Pope. *Turbulent Flows*. Cambridge University Press, 2010.
- [12] A. Prosperetti and G. Tryggvason. *Computational Methods for Multiphase Flow*. Cambridge University Press, 2009.
- [13] Lewis F. Richardson. The supply of energy from and to atmospheric eddies. *The Royal Society*, 1920.
- [14] W. Schröder. Fluidmechanik. lecture notes 'Fluid mechanics', 2010.

- [15] C. Siewert. *Numerical Analysis of Particle Collisions in Isotropic Turbulence*.  
PhD thesis, RWTH Aachen University, 2014.

## 10 Appendix A

### Creating of pictures showing tubular structures

The pictures used in the Introduction were generated using ParaView, an open-source-software developed by a joint-venture of Kitware and the Los Alamos National Laboratory. More information about the software can be found at [www.paraview.org](http://www.paraview.org). To show the tubular structures in a turbulent flow, two filters were used: One was the AIALambda2Criterion1-Filter and the other one was the ISOVolume1-Filter. These filters were then set to visualize the velocity of the flow colored by magnitude. To diversify the different velocity-magnitudes, a rainbow-colorscheme was used.